Journal of Physics: Conference Series **180** (2009) 012057 doi:10.1088/1742-6596/180/1/012057

Whole-volume integrated gyrokinetic simulation of plasma turbulence in realistic diverted-tokamak geometry

C S Chang[1], S Ku[1], P Diamond[2], M Adams[3], R Barreto[4], Y Chen[5], J Cummings[6], E D'Azevedo[4], G Dif-Pradalier[2], S Ethier[7], L Greengard[1], T S Hahm[7], F Hinton[8], D Keyes[3], S Klasky[4], Z Lin[9], J Lofstead[10], G Park[1], S Parker[5], N Podhorszki[4], K Schwan[10], A Shoshani[11], D Silver[12], M Wolf[10], P Worley[4], H Weitzner[1], E Yoon[7] and D Zorin[1]

[1] Courant Institute of Mathematical Sciences, New York University, NY 10012, USA
[2] University of California at San Diego, La Jolla, CA 92093, USA
[3] Columbia University, New York, NY 10027, USA
[4] Oak Ridge National Laboratory, Oak Ridge, TN 37831, USA
[5] University of Colorado at Boulder, Boulder, CO 80309, USA
[6] California Institute of Technology, Pasadena, CA 91125, USA
[7] Princeton Plasma Physics Laboratory, Princeton, NJ 08543, USA
[8] Hinton Associates, Escondido, CA 92029, USA
[9] University of California at Irvine, Irvine, CA 92697, USA
[10] Georgia Institute of Technology, Atlanta, GA 30332, USA
[11] Lawrence Berkeley National Laboratory, Berkeley, CA 94720, USA
[12] Rutgers University, New Brunswick, NJ 08901, USA

E-mail: cschang@cims.nyu.edu

Abstract. Performance prediction for ITER is based upon the ubiquitous experimental observation that the plasma energy confinement in the device core is strongly coupled to the edge confinement for an unknown reason. The coupling time-scale is much shorter than the plasma transport time-scale. In order to understand this critical observation, a multi-scale turbulence-neoclassical simulation of integrated edge-core plasma in a realistic diverted geometry is a necessity, but has been a formidable task. Thanks to the recent development in high performance computing, we have succeeded in the integrated multiscale gyrokinetic simulation of the ion-temperature-gradient driven turbulence in realistic diverted tokamak geometry for the first time. It is found that modification of the self-organized criticality in the core plasma by nonlocal core-edge coupling of ITG turbulence can be responsible for the core-edge confinement coupling.

1. Introduction

In order to achieve the design goal of Q=10 (fusion output energy/input energy), ITER[2] relies upon the so called high-mode (H-mode) plasma operation in which an edge temperature pedestal is formed as the core heating power is increased. For an unknown reason, transition into H-mode is accompanied with an instantaneous improvement of the core turbulence level and ion

temperature. The time scale of this core-edge coupling is much faster than the core-edge energy transport time scale. Moreover, the overall ion temperature T_i gradient becomes stiff, raising the core T_i as the edge pedestal T_i value grows while keeping it low in the scrape-off layer. Since the scrape-off layer plasma touches the material wall, its temperature must be kept cool in order to minimize the damage to the material wall. Without the edge pedestal effect in H-mode operation, it is difficult to keep the scrape-off layer plasma cool while raising the core temperature. These H-mode phenomena (formation of edge pedestal and the simultaneous improvement of the core plasma temperature) are crucial ubiquitous experimental findings which have been making the thermonuclear fusion program brighter. However, a satisfactory theoretical understanding of these critical core-edge coupled phenomena is still absent, and awaits an integrated micro-turbulence and neoclassical simulation of core-edge plasmas in a realistic device geometry.

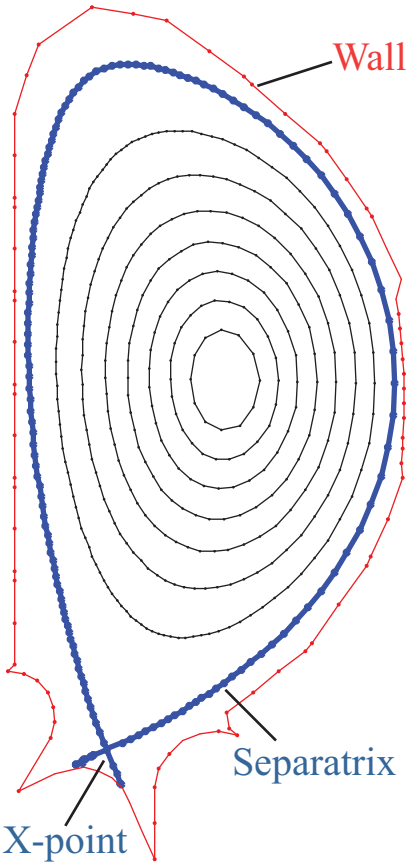

Figure 1. Magnetic flux surfaces of diverted tokamak geometry in a poloidal plane. X-point is shown on the separatrix. ITER is used as an example.

Although the necessity has thereby been recognized for a long time, it is a formidable challenge to capture both edge and core regions in an integrated global simulation. The difficulty of this problem is further exacerbated by the geometric complexity introduced in the edge region by the presence of a divertor and, thus, the magnetic separatrix surface (see Fig. 1). The magnetic separatrix surface is a singular surface to the conventional "flux" coordinate system used in the existing gyrokinetic codes. Due to this reason, the existing gyrokinetic codes do not approach the magnetic separatrix surface. At the same time, the existence of the magnetic X-point on the separatrix surface and an arbitrary wall shape in a tokamak device makes the conventional tokamak gyrokinetic mesh inadequate and requires a specially designed, field-line

following unstructured mesh (see Fig. 2). This poses extra difficulties in the gyrokinetic particle simulation of diverted edge plasma. Details of the mesh property used in XGC1 can be found in the paper by M. Adams, S. Ku et al., presented at this conference [1]. In the present work such a geometrically difficult simulation challenge is combined with the formidable non-local, nonlinear, multi-scale physics challenges on a) a first-principles global gyrokinetic simulation to capture the basic physics of the nonlocal turbulence coupling and associated transport; b) a full distribution function representation (full-f) implemented to properly take into account the loss of single particle confinement across the magnetic separatrix surface and the formation of a strong edge ExB shearing layer thereby; and c) a multi-scale integrated modeling approach which includes the neoclassical physics together with the turbulence physics as demanded by a proper self-consistent evolution of the global core-edge background profile in the presence of nonlinear turbulence propagation and turbulence-driven transport. The full-f equation described here is different from the conventional full-f representation used in other fields in that the distribution function is reduced from the conventional six dimensional phase space to five dimensional phase space based upon the fast gyromotion perpendicular to the strong background magnetic field (leading to 5D gyrokinetic equation [17]). Eventhough it is a reduced equation from the conventional full-f equation, such a "full-f" global 5D gyrokinetic simulation in realistic magnetic geometry represents a major technical challenge that demands extreme scale computing resources.

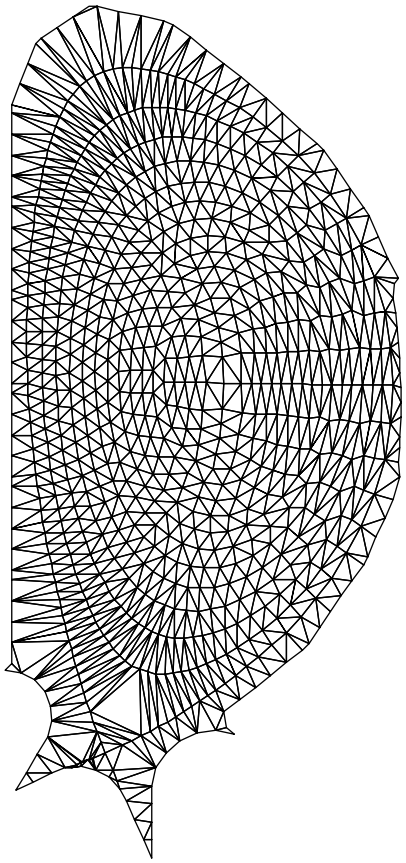

Figure 2. A sample unstructured triangular mesh with diverted magnetic field. The actual scale of the grid used in the simulations is approximately 30 times finer. ITER is used as an example.

Representative micro-turbulence phenomena in tokamak plasma are driven by the ion

temperature gradient (ITG), electron temperature gradient (ETG), trapped electron drift resonance (TEM), magnetic field gradient (Ballooning Modes), and other instabilities. Among them the electrostatic ITG turbulence is the most fundamental one, setting the baseline turbulence transport at the longer wavelength scale. Other turbulence drivers change or add the micro-fluctuation and transport properties. In the present work, we include the ITG turbulence only, as a first step toward the formidable challenge. Other turbulence modes are to be added in the future as the computing power and the numerical technique improve further.

The "full-f" gyrokinetic code (XGC1) in the CPES project has been successfully developed targeting the difficulties noted in diverted edge geometry and the integrated nonlocal physics between turbulence and neoclassical physics (see Ref. [7], Invited Paper, 2008 American Physical Society, Division of Plasma Physics). Thanks to the recent petascale capability of ORNL's *Jaguar* computer and the generous award in the 2009 INCITE and OASCR/OFES Joule programs, XGC1 computing has been pushed to the extreme limit where no other gyrokinetic code has ever approached. Ion temperature gradient (ITG) driven turbulence physics has been simulated in integration with the background neoclassical physics using full-f gyrokinetic ions and adiabatic electrons. The simulation volume has been extended to the entire toroidal plasma volume (corresponding to the DIII-D tokamak facility at General Atomics) – from the magnetic axis to the material wall and across the mathematically complex magnetic separatrix region. Central plasma heating and conserving Coulomb collisions are also taken into account to make the simulation more realistic. One production run in DIII-D geometry consumes about 1.5M MPP hours, which is equivalent to the operation of 150,000 *Jaguarpf* XT5 cores for 10 hours in the well-scaled XGC1 simulation. The excellent scalability of XGC1 to petascale computing is, as reported in Ref. [1], shown in Fig. 3.

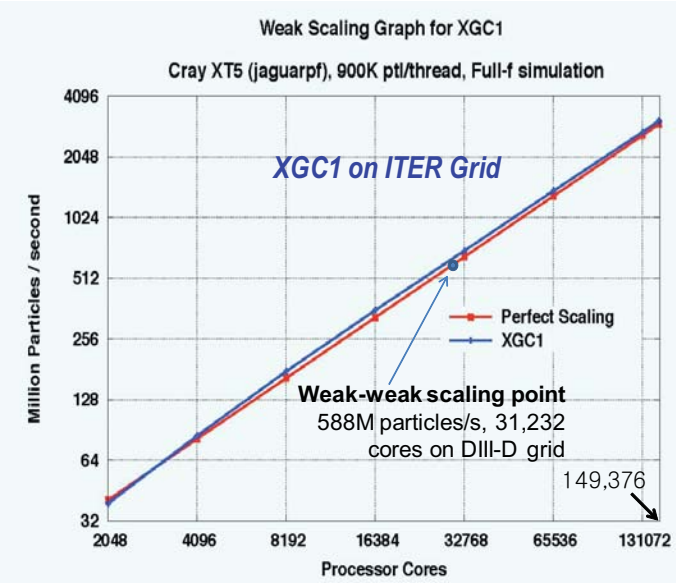

Figure 3. Two different weak scalings on fixed ITER grid (weak-strong) and on two different device grids (weak-weak, ITER vs DIII-D). Both of them show excellent scalability.

The purpose of this paper is to report such a high capacity simulation using the XGC1 code and the resulting new physics understanding of how H-mode plasma operation is maintained through nonlocal nonlinear coupling between core and edge plasmas. The paper is organized as follows. After this introduction section, the XGC1 code is described in Section 2. The new physics discovery is presented in Section 3, followed by conclusion and discussion in Section 4.

2. The full-f gyrokinetic code XGC1

XGC1 is a full-f gyrokinetic particle-in-cell code [6, 7] which can simulate the whole plasma volume including the magnetic axis, the magnetic separatrix and the scrape-off layer bounded by a biased material wall, by reading in a g-eqdsk data file generated from experimental equilibrium reconstruction [16]. XGC1 in its present form is an electrostatic code. Full-f marker ions and adiabatic electrons are used in the present study of ITG turbulence. A heat source is placed in the central core plasma to induce a heat flux into the simulation region, achieved by raising the particle kinetic energy in the source region by a small fraction while keeping the pitch angle invariant. The heat is then lost to the materal wall by self-consistent transport. A heat source is necessary to maintain the plasma in a self-organized global profile. A particle-, momentum- and energy-conserving linear Monte Carlo Coulomb collision operator is built into the particle motion [5, 23, 25, 10, 18]. Monte Carlo neutral particles can also be simulated together in the full-f XGC family codes [5]. In the present short-time simulation, however, the neutral particle routine is not used.

Marker particles follow the electrostatic Lagrangian equation of motion which conserves the mass, the canonical angular momentum and the energy [24, 4, 19].

$$\begin{aligned} \dot{\mathbf{X}} &= (1/D)[v_\parallel \hat{b} + (v_\parallel^2/B)\nabla B \times \hat{b} + \{\mathbf{B} \times (\mu \nabla B - \mathbf{E})\}/B^2] \\ \dot{v_\parallel} &= -(1/D)(\mathbf{B} + v_\parallel \nabla B \times \hat{b}) \cdot (\mu \nabla B - \mathbf{E}) \\ D &= 1 + (v_\parallel/B)\ \hat{b} \cdot (\nabla \times \hat{b}), \end{aligned} \tag{1}$$

where $v_\parallel$ is the speed of the particle parallel to the local magnetic field vector $\mathbf{B}$, $\hat{b} = \mathbf{B}/B$, $\mu = v_\perp^2/2B$ is the magnetic moment, and $\mathbf{E}$ is the gyro-averaged electric field. XGC1 uses a cylindrical coordinate system for the particle advance, which allows particle motion in true arbitrarily shaped flux surfaces including the magnetic separatrix and X-point. In a conventional magnetic flux coordinate system, the equation of motion encounters a mathematical singularity on the magnetic separatrix surface, and the error in the particle motion grows rapidly as it approaches the magnetic separatrix.

The following gyrokinetic Poisson equation is solved on a mesh with the four-point averaging technique [21],

$$-\nabla_\perp \frac{\rho_i^2}{\lambda_{Di}^2} \nabla_\perp \Phi = e\left(1 - \nabla_\perp \rho_i^2 \nabla_\perp\right)(\overline{n}_i - n_e), \tag{2}$$

where $\rho_\mathbf{i}$ is the ion gyroradius vector, λ_{Di} is the ion Debye length, and $\overline{n}_i$ is the ion density in real space [17],

$$\overline{n}_i = \frac{1}{2\pi} \int f_i(\mathbf{X}, \mu, u)\delta(\mathbf{X} - \mathbf{x} + \rho_\mathbf{i}) d\mathbf{X} d\mu d\alpha,$$

$\mathbf{x}$ is the particle position vector, and α is the gyro-phase angle. The above gyrokinetic Poisson equation is valid for steep gradient plasma, too, as long as the plasma gradient scale length is much greater than the ion gyroradius.

In order to take advantage of the slowly varying nature of the electric potential (both neoclassical and turbulent) along the magnetic field lines, the electrostatic potential is solved on an approximately field-line following mesh as is usually done in the conventional turbulence codes. Meshes on all the ploidal planes are identical (axisymmetric) in XGC1. When a mesh node is mapped along the magnetic field line, it approximately meets another mesh node on the adjacent poloidal plane. The mapping is only approximate because a magnetic field line is not closed unless it is on a mode rational surface. Due to the existence of the magnetic X-point, large flux volume expansion along the field lines, and an arbitrary wall shape, an unstructured triangular mesh system is used in the radial-poloidal plane (and a regular mesh is used in

the toroidal direction). Use of the cylindrical coordinate system for particle advances and the unstructured mesh for the field-line following Poisson solver is necessary in the diverted geometry simulation, but adds complexity and demands an extreme high performance computing (HPC) resource. Details on the innovative numerical approach to these issues can be found in Ref. [1].

The macroscopic physical quantities associated with the guiding center particles in a volume ΔV are defined as follows. f_i, n_i, m_i, $q_{i\psi}$, χ_i are the distribution function, the density, the mass, the heat flux in ψ space, and the thermal conductivity of the guiding center ions, respectively. Radial particle flux is zero in the present adiabatic electron model. The volume can be defined as a flux shell for flux surface averaged quantites, or the local cell for local quantities.

$$f_i(X, v_\parallel, \mu) = (1/\pi\Delta V) \sum_{X_j \in \Delta V} w_j \delta(X - X_j)\delta(v_\parallel - v_{\parallel j}\delta(\mu - \mu_j) \tag{3}$$

$$\begin{aligned}
W &= \sum_{X_j \in \Delta V} w_j \\
n_i &= = W/\Delta V \\
u_\parallel &= \sum_{X_j \in \Delta V} v_{\parallel j} w_j / W \\
T_i &= \frac{1}{3} \sum_{x_j \in \Delta V} w_j m_i \left(2B\mu + \left(v_{\parallel j} - u_\parallel\right)^2\right) / W \\
q_{i\psi_N} &= (1/2) \sum_{X_j \in \Delta V} m_i \left(2B\mu + (v_{\parallel j} - u_\parallel)^2\right) w_j \dot{\vec{X}}_j \cdot \nabla\psi / W \\
\chi_i &= q_{i\psi} / (|\nabla\psi|^2 \frac{\partial T}{\partial \psi})
\end{aligned} \tag{4}$$

Advantages in a full-f particle simulation, in comparison with the conventional delta-f particle simulation [11, 22], are in the ability to calculate the large dynamical variations of the mean and the perturbed parts of the plasma together without scale separation, in the facilitation of sources and sinks, and in the non-growth of the marker particle weights. A full-f particle simulation solves the $df/dt = C(f) + S$ equation directly in a gyrokinetic form, where C is the collision operator and S represents the sources and sinks, by following the guiding center particle motion (Eq. 1) in 5D phase space in the electric field given by Eq. (2). Unlike a delta-f gyrokinetic equation, which requires the conservation of phase-space volume, a full-f simulation can accept a source (sink) model on the right-hand side. There is no scale separation in the dynamical self-organization between the background and the perturbed plasma dynamics, and there is no need to use a fixed Maxwellian temperature profile for a free energy source, as assumed in a conventional delta-f simulation. On the other hand, the simulation is more expensive computationally. A full-f gyrokinetic particle-in-cell code requires many more marker particles, roughly by a factor $\sim (n/\delta n)^2$, than a delta-f gyrokinetic code. Fortunately, the simulation can be carried out without suffering from the monotonic growth of the particle weights as in a delta-f code. The actual number of full-f marker particles used in this study will be discussed in a later section.

XGC1 has been thoroughly verified for the accuracy of the single particle motions by examining the conservation properties, the solver capability in steady state using a simplified manufactured solution method, the collisional neoclassical physics by comparing with known analytic solutions, and the delta-f GAM and linear/nonlinear ITG physics by comparing with other global codes. A method of manufactured solution approach for the turbulence solution

verification is under development by our mathematical and physics team members not only for XGC1 but also for other turbulence codes.

The large amount of physics data I/O from full-f simulation in extreme scale HPC is another challenge XGC1 encounters. A new adaptive I/O library called *ADIOS* has been created to meet this challenge [20]. A factor of 30 improvement in the write speed has been achieved in XGC1, allowing for more frequent write-out of the simulation data for code restart and the real-time physics analysis. Further improvement of *ADIOS* is being made as XGC1 pushes the HPC computing to a higher dimension. The simulation data is moved to the *eSimMon* Dashboard [3], created by our team, using the Kepler workflow engine in our EFFIS (End-to-end Framework for Fusion Integrated Simulation) framework for physics analysis including vector graphics and movie viewing.

3. Full-f simulation of whole-device ITG turbulence

We load the marker particles initially as a local Maxwellian, with flux-function density and temperature profiles (the magnetic flux-surface label, such as the enclosed poloidal magnetic flux ψ, is usually used as a radial coordinate). Instead of using the marker particle density to describe the radial profile of the plasma number density, we use the particle weight distribution as a function of radius. To be more specific, the particle weight distribution w_j in Eq. (3) is initialized with ψ_N dependence, where ψ_N is the poloidal magnetic flux normalized to be zero on the magnetic axis and unity at the separatrix surface. This method can resolve the enhanced particle noise problem at the low density region of the plasma profile. The particle weight in the simulation is normalized to unity at the magnetic axis, decreasing in minor radii according to the initial density profile (variation in the particle weight is normally within factor of 10). The experimental particle density is then represented by another normalization.

We note here that the local Maxwellian loading in the laboratory frame contains some unspecified initial toroidal rotation in an inhomogeneous plasma, which is physically insignificant compared to other free energy sources (such as the radial pressure gradient). Thus, the effect of initially large toroidal rotation on turbulence cannot be studied in the present simulations. A neutral beam type of external momentum source is not considered in the present work either, even though this capability is available in the XGC family code, XGC0.

We could also initially load the marker particles as a global canonical Maxwellian, which may yield more rapid reduction of the initial GAM activities and faster self-organization to the neoclassical solution [15]; hence, an easier growth of turbulence. It is well-known that unless the initial GAM activities are subdued, ITG turbulence does not grow in a full-f simulation [8]. However, the canonical Maxwellian loading has a disadvantage in that it is difficult to customize the radial temperature and density profiles. For this reason, we choose the local Maxwellian loading to take advantage of the easier profile customization. We get compensation for the disadvantage by obtaining a neoclassical radial electric field solution in a pre-conditioning simulation and using it in the turbulence simulation as the initial electric field. Since the particle loading after the preconditioning run is still a local Maxwellian, this process does not eliminate the initial GAM oscillations completely, but helps reduce the amplitude and the relaxation time.

The boundary condition we use on the elliptic Poisson equation is that the electrostatic potential on the material wall surface vanishes. Any particle hitting the wall surface is absorbed to the wall and removed from the simulation. Initial plasma profiles are shown in Fig. 4. The initial ion temperature T_i at the magnetic axis is chosen to be 4.5 keV, dropping linearly in $\sqrt{\psi_N}$ ($\propto$ real radius, approximately) to about 1.3 keV at the temperature pedestal top $\psi_N \simeq 0.83$ before following a tanh profile to form the edge pedestal. The relation between the real distance along the outside midplane and ψ_N is given in Fig. 5, together with the safety factor q profile (which is stopped short of the magnetic separatrix surface $\psi_N = 1$ where it becomes infinite). This T_i profile is not far off from experimental observations, and hence yields a realistic ratio

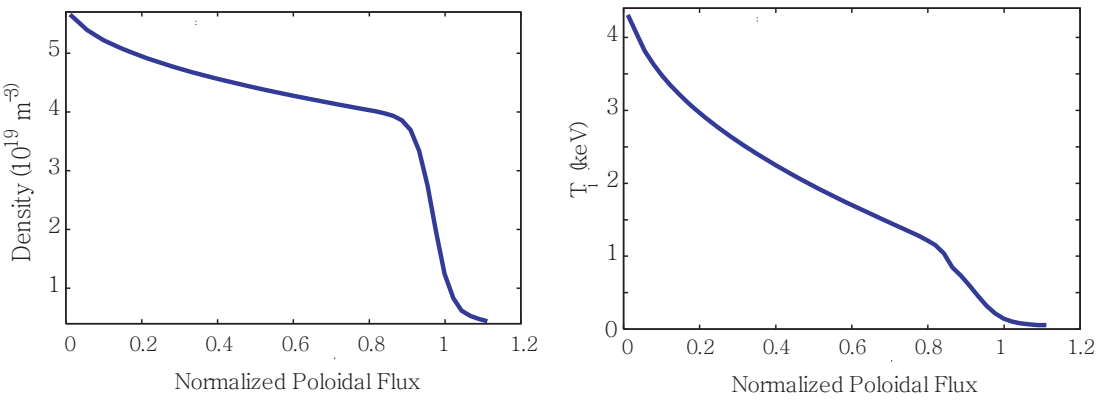

Figure 4. Early-time plasma density and temperature profiles. Electron temperature is assumed to be equal to ion temperature. Notice that the temperature pedestal knee is located at a somewhat smaller minor radius than the density pedestal knee, making the relative temperature slope high between the two knees.

of the ion larmor radius (or the shortest turbulence wave length considered) to the device size ($a/\rho_i \simeq 200$ where $\rho_i \simeq 3$ mm is the average ion gyroradius and $a \simeq 60$ cm is the minor radius along the outside midplane at the material wall of DIII-D). Of course, the initial T_i profile changes with heat transport as the simulation progresses. For a representative value of $v_i = (T_i/m_i)^{1/2}$, where m_i is the deuteron mass, we take $T_i = 4$ keV.

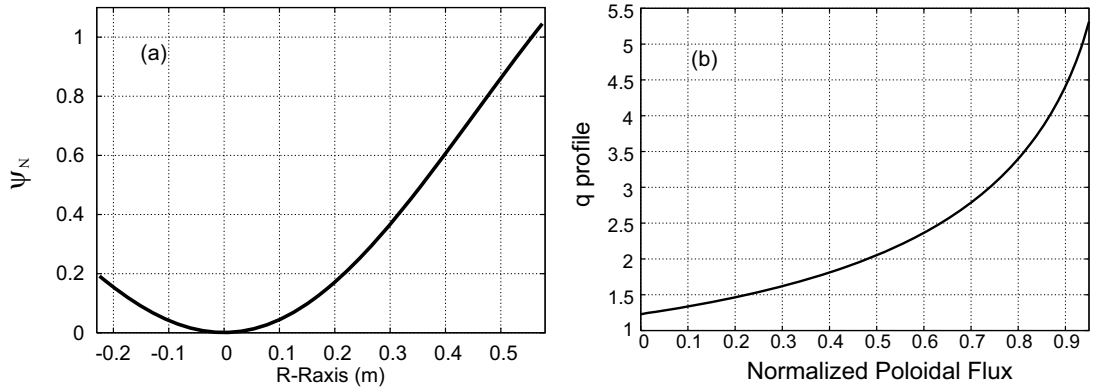

Figure 5. (a) Relationship between the normalized poloidal flux ψ_N and real distance in meters from the magnetic axis ($R_{axis} = R_o$) to the flux surface (R) along the midplane. (b) Radial profile of the safety factor q.

Plasma density n at the magnetic axis is chosen to be $5.5 \times 10^{19} m^{-3}$, dropping to about $4 \times 10^{19} m^{-3}$ at the density pedestal top $\psi_N \simeq 0.9$ with linear dependence in $\sqrt{\psi_N}$, followed by another tanh profile to form a density pedestal. Since we use adiabatic electrons, the plasma density profile does not change in time.

Stability of ion temperature gradient (ITG) modes in the core plasma is usually described in terms of the ratio between the major radius at the magnetic axis R_0 (or R_{axis}) and radial T_i gradient scale length, $R_0/L_T = R_0|\partial \log T_i/\partial r|$. The initial profile of R_0/L_T is as shown in Fig. 6. The horizontal dashed line is the nonlinear stability criterion of a core plasma from

Ref. [9], which is invalid in the edge pedestal [6]. As can be seen in Fig. 6, R_0/L_T is below the nonlinear stability limit in the significant portion of the core plasma $\psi_N < 0.5$ (r/a¡0.6), but rises steeply in the edge pedestal for a stronger ITG drive. As will be shown shortly, this does not mean that the ITG turbulence is strong in the edge pedestal, proving the invalidity of the R_0/L_T criteron there.

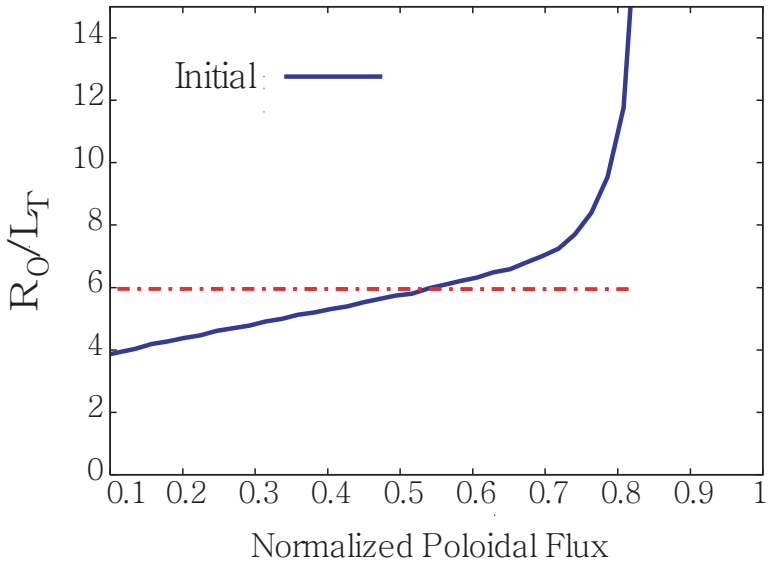

Figure 6. Initial profile of $R_0/L_T = R_0|\partial \log T_i/\partial r|$. The horizontal dashed line is the nonlinear stability criterion of a core plasma, from Ref. [9].

In an H-mode plasma, a strong radial electric field layer forms just inside the magnetic separatrix surface, consistent with a steep density pedestal as observed in experiments in the radial force balance relation. Our previous simulation shows that the formation of the strong radial electric field layer is from the X-point effect (loss of single particle ion confinement) [6]. In the present ITG simulation in H-mode type pedestals, we assume the existence of a reasonably strong edge density pedestal profile. The radial electric field and the sheared flows are then evaluated in the code self-consistently with the neoclassical and turbulence physics. Since our turbulence model uses adiabatic electrons, the plasma density profile does not evolve. Only the ion temperature T_i profile evolves. The electron temperature profile is assumed to be equal to the ion temperature profile.

The temperature and density profiles are within a realistic range of experimental values in DIII-D. However, in order to save the computing time, we artificially enhance the collision frequency by a factor of 10 (yielding the average ion collision time to be $\tau_{ic} \simeq 140\ v_i/R$). The simulation is then performed to a few collision times. Not only the neoclassical relaxations, but also the GAM and zonal flow relaxation become faster in proportion to collision frequency. A factor of 10 enhancement of the collision frequency still keeps the plasma in the banana regime all the way out to the pedestal top ($\nu_* = 0.7$ at $\psi_N = 0.83$), keeping the integrity of the particle orbit dynamics.

Convergence tests in marker particle number have been performed up to 12 billion particles and have revealed that a total of 5 billion marker particles (average $\sim$ 2,000 marker particles per grid node) is minimal for an adequate study of the global ITG turbulence. This yields a noise driven χ_i at the level $\simeq 0.05\ m^2/s$, which is identified from the simulations performed without ITG or collisions and is much lower than the χ_i level ($\gtrsim 1m^2/s$) obtained in the actual

simulation with ITG turbulence and enhanced collisions. Convergence tests in the grid size show that we need $\simeq 3\ mm$ average grid size at the outside midplane, which is about the average ρ_i size. We have used various numbers of *Jaguarpf* XT5 cores (up to 149,760) for benchmarking and scaling studies. The actual simulation results presented here are from 7.5 billion marker particles (corresponding to an average of $\sim$ 3,000 marker particles per grid node) run for 88 hours on 14,976 CRAY XT5 cores to obtain a relatively steady ion heat flux or turbulence level (corresponding to a total of 2.4 ms in real time). This corresponds to about 10 hours with 149,760 XT5 cores (the full capacity of *Jaguarpf*), taking into account some performance degradation. A weak scaling study of XGC1 up to 149,760 cores is presented in Ref. [1].

The time step of the simulation ($= 0.04\ R_0/v_i$) is chosen from a convergence test. The number of total time steps taken in the simulation presented here is 10,000.

4.5MW of total heat is added to the ions around the magnetic axis ($\psi_N \leq 0.04 \simeq 10cm$) to force a heat flux into the turbulence region. The heating is achieved by raising the particle energy uniformly in the heating region by a small fraction of the kinetic energy while keeping the pitch angle invariant. This rate of heating in a small central volume is too large for the local ITG and neoclassical transports to efficiently transport the heat radially outward. As a matter of fact, the full-f plasma even shows resistance to the local heat flux by developing a strong E $\times$ B shearing rate in the heat source region. In order to ensure a smooth outward heat flux from the localized heating, we raise further the Coulomb collision rate by another factor of 10 (thus raising the neoclassical transport level) in the central core ($\psi_N \leq 0.08 \simeq 13cm$) in a somewhat greater volume than the heat source volume. This artifical collision is part of the central heating model in the code.

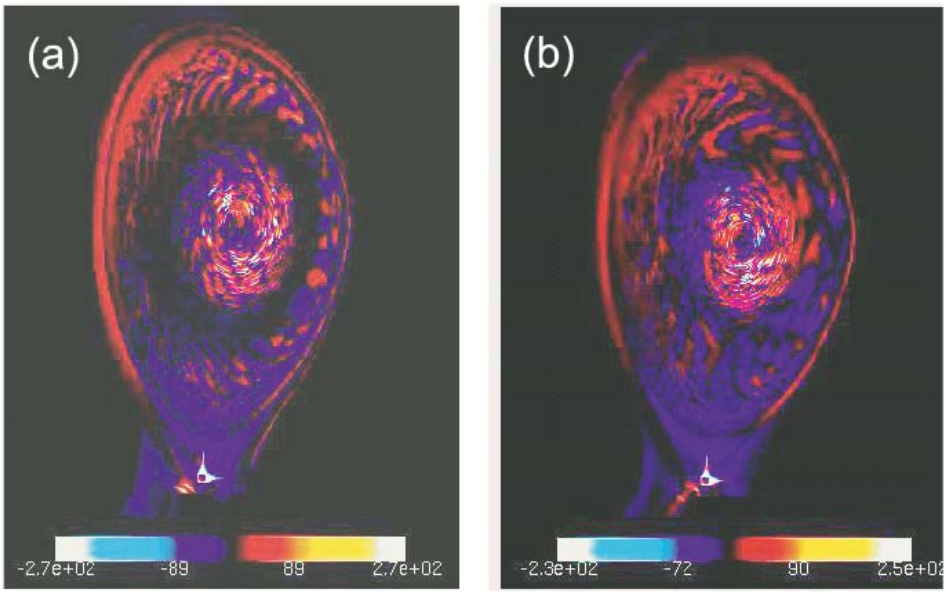

Figure 7. Snapshot figures of turbulent electrostatic potential on a poloidal (constant toroidal angle) plane at an (a) early and (b) later stage

Figure 7 shows two snapshots of fluctating electrostatic potential contour on the poloidal cross-section in the earlier and later phases of the ITG turbulence. It can be clearly seen that the turbulence starts at two places: in the edge where R_0/L_T is large and in the central core where the heating source exists. A dark ring just inside the separatrix surface indicates weak turbulence intensity there, even though R_0/L_T is very large there, which is a characteristic

of an H-mode plasma. The edge-generated turbulence propagates radially inward. On the other hand, the heating-generated central turbulence does not propagate outward. It can be seen that the central core turbulence is under a strong (sheared) poloidal rotation, indicating a self-containment of the heating-generated turbulence. The inward propagation stops when the edge-originated turbulence meets the strongly-sheared central turbulence at $t \simeq 150R/v_i$ ($\simeq 0.6$ ms).

Another remarkable observation made from the present simulation is the self-organizing modification of the background temperature profile by the incoming turbulence, as can be seen in Figure 8. Before the arrival of the edge-originated turbulence in the core plasma, the ion temperature gradient was below the nonlinear ITG criticality level (dotted horizontal line, originated from Ref. [9]). However, the arrival of the edge-generated turbulence raises the local temperature gradient above the nonlinear criticality level. The ion thermal conductivity is self-regulated by the self-generated ExB shearing. In other words, the turbulence criticality is nonlocally self-organized by the edge turbulence source. This state is maintained by the outward-flowing heat flux. The combination of the low thermal conductivity near the magnetic separatrix surface and the large heat flux from the core maintains the T_i pedestal and keeps the R_0/L_T around the T_i knee well above the nonlinear criticality level, continuously supplying the ITG turbulence energy to maintain the new self-organized criticality. Without the strong heat flux from the core, the R_0/L_T value around the intitial T_i knee location would collapse, and the driver for the elevated SOC state would be lost. We have examined a few different heating power levels. It is found that the η_i profile shown here is "stiff" with respect to the change of heating power, which is consistent with the experimental findings.

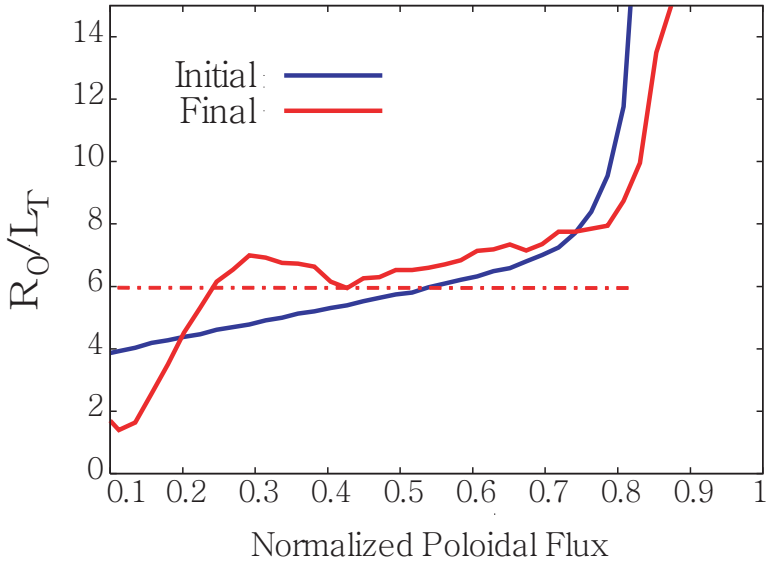

Figure 8. Self-organizing modification of the background temperature profile by the incoming turbulence. The horizontal line represents the nonlinear criticality in the core plasma [9].

Maintaing the T_i knee with a strong heat flux H can be understood in a simple one-dimensional argument as follows: As long as the heat diffusion is the dominant mechanism in determining the temperature gradient (over other energy dissipation or off-diagonal transport mechanisms), the continuity of heat fluxes between two adjacent positions x_1 and x_2 (with $x_1 < x_2$) demands $H = -\chi_1 \partial T_i(x_1)/\partial x = -\chi_2 \partial T_i(x_2)/\partial x$. If χ_2 is forced to stay low for some reason at a high heat flux, $\chi_1 > \chi_2$ results in a strong knee in the T_i profile somewhere between

x_1 and x_2. In the present problem, the strong edge effects (the magnetic separatrix with X-point, strong ExB shearing, and steep density gradient) keep the ITG driven χ_2 low. In the meantime, the high heat flux from the core and the strong ITG maintains a high χ_1 value.

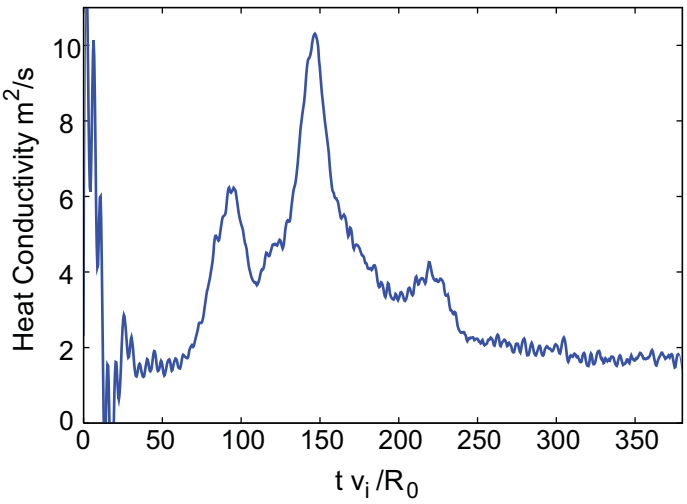

Figure 9. Time behavior of the effective ion thermal conductivity (thermal flux divided by local T_i gradient) from the start of the simulation across $\psi_N = 0.64$ which corresponds to $r = 42$ cm on the outside midplane. The self-organizing process is bursty.

Figure 9 is the time behavior of the effective ion thermal conductivity (thermal flux divided by local T_i gradient) from the start of the simulation across $\psi_N = 0.64$ which corresponds to $r = 42$ cm on the outside midplane. The short initial jittering is driven by GAM oscillations during the self-organization of the radial electric field, ion distribution function, plasma profile, and toroidal rotation toward neoclassical equilibrium in the initial local Maxwellian loading, and is subdued at about 30 v_i/R. At about 60 v_i/R, ITG modes start to grow. As mentioned in the previous section, it is well-known that unless the jittering from the initial GAM activities is subdued, ITG turbulence does not grow in a full-f simulation [8]. The total simulation time is about twice the collision time.

Figure 9 also shows that after the arrival of the turbulence front, there is a distinctive bursty type of heat flux behavior in the initial stage of nonlinear turbulent transport until about 240 v_i/R, as the initial neoclassical ion temperature profile and turbulence are self-organizing, followed by a relatively steady level of heat flux behavior. The inter-burst period is much greater than the initial GAM period. The self-organization process from one global state to another is of interest (such as the transition process from a low to a high mode in a tokamak plasma). The case studied here corresponds to a global transition from a neoclassical state to a turbulent state. The radial speed of the ballistic motion of heat burst is about $V_r \simeq (1/5)\rho_i v_i/R \simeq (1/30)\ \rho_i v_i/L_T)$, which is similar to the analytic estimate of the turbulence intensity propagation speed reported in Refs. [14, 13, 12]. Distinction between the $\rho_i v_i/R$ and $\rho_i v_i/L_T$ scalings in V_r is difficult to determine in the present simulation since R/L_T quickly self-organizes to a fixed value $\simeq 6.5$.

The inward propagation of the bursty turbulence intensity interplays with the local temperature gradient and ExB shearing dynamics. Arrival of the turbulence front at a location is first noticed by the steepening of the local temperature gradient, followed by the increase of heat flux ($\propto$ turbulence intensity) which weakens the temperature gradient, and then followed by increase in the local ExB shearing rate. There is about $\tilde{>} 30 v_i/R_0$ time delay between three local events. Increase of the local ExB shearing rate then suppresses the turbulence and the

outward heat flux, ending the burst. The local temperature steepens again, and the bursty cycle continues until a quasi steady avalanche turbulence is reached at the end, where the turbulence shows a 1/f power law.

In the central core, strong heat source maintains strong E × B shearing (see Fig. 7). As a result, the bursty heat flux does not appear there. It can also be noticed that the ion temperature gradient remains subcritical even though there is a strong turbulence there, indicating that the turbulence is driven by heating, not by the ion temperature gradient. This phenomenon has not been understood, yet. This subject may have an interesting relation to another uniquitous experimental observation that auxilary heating degrades tokamak core confinement. Possible relation of the local heating-driven strong ExB shearing is another interesting topic to be studied in the future, especially in a reversed-q magnetic equilibrium.

Energy conservation has been investigated within the volume $0.3 \leq \psi_N \leq 0.7$. Amongst the energy flowing into the volume across the inner surface $\psi_N = 0.3$, the sum of the particle energy change, the field energy created, and the outward-flowing energy across the outer surface $\psi_N = 0.7$, the total energy conservation showed about a 2% error. The energy conservation error in a full-f code should not grow unless numerical errors grow.

4. Conclusions and discussions

A special full-f gyrokinetic particle code XGC1 has been developed for a formidable integrated simulation, for the first time, of the core-edge and the neoclassical-turbulence physics in a realistic tokamak geometry including the magnetic separatrix. Turbulence studied in this report is from the electrostatic ITG mode using adiabatic electrons. Central heating is used to drive radial heat flux in the turbulence. A particle number, momentum and energy conserving Monte-Carlo collision operator is used to produce proper collision effects in neoclassical and turbulence physics.

Thanks to the capability computing enabled by the DOE Leadership Class computing systems, new understandings in the ITG turbulence physics are obtained on a) how the core ITG turbulence and ion temperature are instantaneously influenced by the edge plasma condition in a time scale much shorter than the energy confinement time scale and b) how a transition from a neoclassical state to a turbulent state is achieved.

The present numerical study shows strong evidence that the so-called "tail-wagging-dog" phenomenon, as ubiquitously observed in the experiments, can be explained from fast propagation of ITG turbulence energy from the pedestal top to the core and its modification of the core turbulence criticality through nonlocal, nonlinear self-organization. In order to validate and confirm this theoretical finding, an experimental study of the inward ITG turbulence propagation at the L-H transition from the edge pedestal top to the core is strongly suggested.

We note here again that the simulation presented here is only the first step toward understanding the L-H confinement physics in a tokamak. The ITG turbulence study reported here is only electrostatic without particle transport, in fixed magnetic equilibrium, and without turbulence interaction with plasma current. Addition of kinetic electrons and electromagnetic effects, including tearing modes, to the XGC1 turbulence study is the nearest term improvement goal. A routine to evolve magnetic equilibrium and q profile along with the background plasma profile evolution is already incorporated in the sister code XGC0 and will be used in XGC1. Other routines readily available from XGC0 include toroidal torque source and Monte Carlo neutral transport and recycling. Analytic model magnetic ripple capability is already incorporated into XGC1.

Acknowledgments

The XGC1 full-f gyrokinetic code has been developed collaboratively in the SciDAC FSP Prototype Center for Plasma Edge Simulation (CPES), which has been funded by the U.S.

Department of Energy, jointly between the Office of Fusion Energy Science and the Office of Advanced Scientific Computing Research.

This research used resources of the National Center for Computational Sciences at Oak Ridge National Laboratory, which is supported by the Office of Science of the U.S. Department of Energy under Contract No. DE-AC05-00OR22725. The extreme computing on *Jaguarpf* presented here was possible through the 2009 OASCR Joule Milestone program. The authors are indebted to Dr. D. Kothe, K. Roche, R. Kendall and other staff members at NCCS for their help in getting large-size Joule runs on *Jaguarpf*. This research also utilized *Franklin* at NERSC througn ERCAP allocation, also supported by US DOE Office of Science.

The research of D'Azevedo, Klasky, Podhorszki, and Worley was performed at the Oak Ridge National Laboratory, which is managed by UT-Battelle, LLC under Contract No. De-AC05-00OR22725. Accordingly, the U.S. Government retains a nonexclusive, royalty-free license to publish or reproduce the published form of this contribution, or allow others to do so, for U.S. Government purposes.

References

[1] M. Adams, S. Ku, P. Worley, E. D'Azevedo, J. Cummings, and C.S. Chang. *SciDAC2009, submited to J. Phys: Conf. Series.*
[2] R. Aymar, V.A. Chuyanov, M. Huguet, Y. Shimomura, ITER Joint Central Team, and ITER Home Teams. *Nucl. Fusion*, 41:1301, 2001.
[3] R. Barreto, S. Klasky, P. Podhorszki, P. Mouallem, and M. Vouk. *2009 International Symposium on Collaborative Technologies and Systems (CTS 2009).*
[4] A.H. Boozer. *Phys. Fluids*, 27:2441, 1984.
[5] C. S. Chang and S. Ku. *Phys. Plasmas*, 11:2649, 2004.
[6] C. S. Chang and S. Ku. *Phys. Plasmas*, 15:062510, 2008.
[7] C. S. Chang, S. Ku, P. Diamond, Z. Lin, S.Parker, T.S. Hahm, and N. Samatova. *Phys. Plasmas*, 16:056108, 2009.
[8] G. Dif-pradalier, V. Grandgirard, Y. Sarazin, X. Garbet, Ph. Ghendrih, and P. Angelino. *Phys. Plasma*, 15:042314, 2008.
[9] A. M. Dimits, G. Bateman, M. A. Beer, B. I. Cohen, W. Dorland, G. W. Hammett, C. Kim, J. E. Kinsey, M. Kotschenreuther, A. H. Kritz, L. L. Lao, J. Mandrekas, W. M. Nevins, S. E. Parker, A. J. Redd, D. E. Shumaker, R. Sydora, and J. Weiland. *Phys. Plasmas*, 7:969, 2000.
[10] A. M. Dimits and B. I. Cohen. *Phys. Rev. E*, 49, 1994.
[11] A. M. Dimits and W. W. Lee. *J. Comput. Phys.*
[12] X. Garbet, Y. Sarazin, F. Imbeaux, P. Ghendrih, O. D. Gurcan C. Bourdelle, and P. H. Diamond. *Phys. Plasmas*, 14:122305, 2007.
[13] D. Gurcan, P. H. Diamond, and T. S. Hahm. *Phys. Plasmas*, 14:055902, 2007.
[14] T.S. Hahm, P.H. Diamond, and Z. Lin. *Phys. Plasmas*, 12:090903, 2005.
[15] Y. Idomura, S. Tokuda, and Y. Kishimoto. *Nucl. Fusion*, 43:234, 2003.
[16] L. L. Lao, H. St. John, R. D. Stambaugh, A.G. Kellman, and W. Pheiffer. *Nucl. Fusion*, 25:1611, 1985.
[17] W. W. Lee. *Phys. Fluids*, 26:556, 1983.
[18] Z. Lin, W. M. Tang, and W. W. Lee. *Phys. Plasmas*, 2, 1995.
[19] R.G. Littlejohn. *Phys. Fluids*, 28:2015, 1985.
[20] J. Lofstead, F. Zheng, S. Klasky, and K. Schwan. *IPDPS 2009, IEEE Computer Society Press*, 2009.
[21] Y. Nishimura, Z. Lin, J.L.V. Lewandowski, and S. Ethier. *J. Comp. Phys.*, 214:657, 2006.
[22] S. E. Parker and W. W. Lee. *Phys. Plasmas*, B5:77, 1993.
[23] W. X. Wang, N. Nakajima, M. Okamoto, and S. Murakami. *Plasma Phys. Controlled Fusion*, 41, 1999.
[24] R. White. *Phys. Fluid B*, 2:845, 1990.
[25] X. Q. Xu and M. N. Rosenbluth. *Phys. Fluids B*, 3, 1991.